Parkinsonism Sac domain mutation in Synaptojanin-1 affects ciliary properties in iPSC-derived dopaminergic neurons

Nisha Mohd Rafiq[a,b,c,d,1,2] (iD), Kenshiro Fujise[a,b,c,d] (iD), Martin Shaun Rosenfeld[a,b,c,d], Peng Xu[a,b,c,d] (iD), and Pietro De Camilli[a,b,c,d] (iD)

Synaptojanin-1 (SJ1) is a major neuronal-enriched PI(4, 5)P₂ 4- and 5-phosphatase implicated in the shedding of endocytic factors during endocytosis. A mutation (R258Q) that impairs selectively its 4-phosphatase activity causes Parkinsonism in humans and neurological defects in mice (SJ1^{RQ}KI mice). Studies of these mice showed, besides an abnormal assembly state of endocytic factors at synapses, the presence of dystrophic nerve terminals selectively in a subset of nigro-striatal dopamine (DA)-ergic axons, suggesting a special lability of DA neurons to the impairment of SJ1 function. Here we have further investigated the impact of SJ1 on DA neurons using iPSC-derived SJ1 KO and SJ1^{RQ}KI DA neurons and their isogenic controls. In addition to the expected enhanced clustering of endocytic factors in nerve terminals, we observed in both SJ1 mutant neuronal lines increased cilia length. Further analysis of cilia of SJ1^{RQ}DA neurons revealed abnormal accumulation of the Ca²⁺ channel Ca$_v$1.3 and of ubiquitin chains, suggesting a defect in the clearing of ubiquitinated proteins at the ciliary base, where a focal concentration of SJ1 was observed. We suggest that SJ1 may contribute to the control of ciliary protein dynamics in DA neurons, with implications on cilia-mediated signaling.

primary cilia | Parkinson's disease | calcium channel | centriole | phosphoinositides

While the cause of most Parkinson's disease (PD) is not known, mutations in a selected list of genes are responsible for the development of familial forms of the disease, often Early-Onset Parkinsonism (EOP) (1). One such gene is *SYNJ1*, which encodes the protein Synaptojanin-1 (SJ1), a polyphosphoinositide phosphatase highly expressed in neurons and enriched at synapses (2–4). SJ1 dephophorylates PI(4, 5)P₂ via the sequential action of two tandemly arranged inositol phosphatase modules: a central 5-phosphatase domain and an N-terminal Sac1 domain which functions primarily as a 4-phosphatase (2, 5, 6). These catalytic modules are followed by a proline-rich region which is responsible for its subcellular targeting and undergoes alternative splicing to generate a shorter (145 kD, the predominant neuronal form) and a longer (170 kD) isoform (2, 7, 8). One of the main known roles of SJ1 is to participate in the shedding from endocytic vesicles of clathrin coats and other endocytic factors, including actin regulatory proteins, which bind PI(4, 5)P₂ at the plasma membrane to initiate the endocytic reaction (9, 10). While the absence of SJ1 leads to early postnatal lethality in mice (9) and humans (11, 12), a patient R258Q missense mutation (SJ1^{RQ}) (accession number: NM_003895) also known as R219Q (accession number: NM_001160302) is responsible for EOP with epilepsy. This mutation selectively abolishes the catalytic action of its Sac1 domain (SJ1^{RQ}) (3). We previously showed that knock-in mice with this mutation (SJ1^{RQ}KI) display neurologic manifestations reminiscent of those of human patients (13). These manifestations are accompanied at the cellular level not only by endocytic defects and an accumulation of clathrin-coated vesicles at synapses but also by degenerative changes selectively of a subset of dopaminergic nerve terminals in the dorsal striatum (13, 14).

One cell compartment which is regulated by PI4P and PI(4, 5)P₂ dynamics is the primary cilium (15–18). PI(4, 5)P₂ in the plasma membrane of the ciliary pocket at the base of the cilium, which is a site of intense exo-endocytosis, helps regulate the turnover of cilia-related signaling proteins (15, 17, 19). Moreover, PI(4, 5)P₂ is the precursor of the pool of PI4P generated in the ciliary shaft through dephosphorylation of PI(4, 5)P₂ by INPP5E, a polyphosphoinositide 5-phosphatase concentrated in the shaft of primary cilia. This PI4P pool has a critical role in cilia biology (17, 18, 20–23). Primary cilia are key players in the hedgehog signaling pathway which has a crucial importance in the nigrostriatal system (24–27). The importance of hedgehog signaling in the development of DA neurons is proven by the essential requirement of Sonic Hedgehog (Shh) for the differentiation of iPSCs into DA neurons (28, 29). Primary cilia of neurons are increasingly recognized as major signaling hub with a major impact on neuronal function. Interestingly,

Significance

A mutation in the catalytic action of Sac1 domain in Synaptojanin-1 (SJ1) causes early-onset Parkinsonism. Here, we show that this mutation affects the characteristics of cilia of induced pluripotent stem cell (iPSC)-derived dopaminergic neurons. Cilia are longer and show an accumulation of calcium channels and ubiquitinated proteins relative to control neurons, suggesting an effect of SJ1 on protein turnover in these organelles. These findings have implications for a link between cilia-mediated signaling to Parkinson's Disease.

disease-causing mutations in another PD gene, LRRK2 (PARK8) (30–34) interfere with ciliogenesis (26, 32, 35), suggesting a potential contribution of ciliary-related defects to PD pathology. While one effect of PD LRRK2 mutations is to impact DA neurons indirectly, via an impairment of cilia-dependent hedgehog signaling in striatal cholinergic neurons (26, 35), additional direct effects of these mutations via an impairment of cilia in DA neurons cannot be excluded. These considerations raise the question of whether phenotypic manifestations of SJ1 impairment may include perturbations of ciliary functions and whether such perturbations may occur in DA neurons.

Here, we have used iPSC-derived DA neurons as a model system to address this question. We report that DA neurons with impaired SJ1 function have abnormally long cilia which display an ectopic accumulation of ubiquitinated proteins within them. The $Ca_v1.3$, a voltage-gated calcium channel, which is important for the rhythmic pacemaking activity of DA neurons (36–39), is also abnormally accumulated within them. Together, our results demonstrate a role of SJ1 in the dynamics of cilia of DA neurons and implicates this protein in the control of their signaling properties.

Results

Generation of WT and SJ1 Mutant iPSC-Derived DA Neurons. Human iPSCs (WTC11 line) were gene edited in house by CRISPR/Cas9 to delete expression of SJ1 (SJ1 KO). Correct editing was validated by PCR and the absence of SJ1 in KO cells was confirmed by western blotting (*SI Appendix*, Fig. S1 *A* and *B*). iPSCs (KOLF2.1 line) harboring the EOP RQ mutation at position 258 (accession number: NM_003895) were obtained from the iPSC Neurodegeneration Initiative (iNDI) (40) and validated by PCR. SJ1 KO and SJ1^{RQ}KI iPSCs as well as their corresponding isogenic controls were differentiated either into cortical-like i^{3}neurons or into DA neurons (*SI Appendix*, Fig. S1 *C–G*). To generate cortical-like i^{3}Neurons, we used the doxycycline-inducible neurogenin-2 (NGN2)-driven differentiation protocol (41) as described in Fernandopulle et al. (42) which results in mature neuronal cultures within 15 to 19 d. For the generation of DA neurons, we used the procedure described by Kriks et al. (28) and Bressan, Dhingra, Donato, and Heutink (43). This differentiation process is slower than the NGN2-driven neuronal differentiation (42–44). However, 30 d from the beginning of differentiation, cells had acquired neuronal morphology with the formation of a complex network of processes (*SI Appendix*, Fig. S1 *C* and *D*). Moreover, western blotting and immunofluorescence of these cultures showed the expression of two key markers of DA neurons, tyrosine hydroxylase, and the dopamine transporter, in both the control and the two SJ1^{RQ}KI mutant lines (*SI Appendix*, Fig. S1 *E–I*).

iPSC-Derived SJ1 Mutant DA Neurons Display Abnormal Accumulation of Endocytic Factors in Nerve Terminals. A key and defining phenotype of SJ1 KO and SJ1^{RQ}KI neurons in situ and in primary cultures is a very robust and exaggerated accumulation in their nerve terminals of endocytic membrane intermediates and endocytic factors, including clathrin coat components and their accessory factors, with amphiphysin-2 being the most strikingly accumulated protein (13). To validate the use of iPSC-derived DA neurons as model systems to assess the impact of SJ1 mutations, we examined whether this phenotype was recapitulated in these cells.

At days 50 to 55 from the beginning of differentiation, SJ1 KO neurons, SJ1^{RQ}KI DA neurons, and their corresponding control neurons showed a similar and prominent punctate pattern of immunoreactivity for the synaptic vesicle marker synaptophysin, revealing abundant formation of synapses in all four conditions. However, a very strong and robust accumulation of puncta of amphiphysin-2 immunoreactivity, which overlapped with synaptophysin immunoreactivity (Fig. 1 *A–F*), was observed in SJ1 KO and SJ1^{RQ}KI DA neurons, but not in control neurons, demonstrating that the accumulation of endocytic factors typical of SJ1 KO neurons (13) is replicated in these iPSC-derived neurons. These accumulations were also seen when SJ1^{RQ}KI DA neurons were cocultured for 7 d with iPSC-derived medium spiny neurons (MSNs) from BrainXell (Fig. 1 *G–J*) using a microfluidic compartmentalization device (eNuvio). In this device, DA neurons and MSNs are seeded in two distinct chambers connected by narrow channels through which axons can grow. Large abnormal puncta of amphiphysin-2 immunoreactivity, which overlapped with puncta positive for synapsin, a marker of presynaptic nerve terminals (45), were observed in both chambers, with the puncta found in the MSN-containing chamber likely reflecting primarily DA synapses on MSNs. We conclude that iPSC-derived DA neurons are good models to study SJ1 mutant phenotypes.

Presence of Primary Cilia in iPSC-Derived DA Neurons and Abnormal Ciliary Length in SJ1 KO and SJ1^{RQ}KI DA Neurons. Cilia brightly positive for the primary cilia marker Arl13b (46) were clearly visible in undifferentiated iPSCs, but no longer detectable after differentiation to cortical-like i^{3}Neurons (Fig. 2 *A* and *B*). This is in agreement with the decrease of the levels of mRNAs encoding cilia-related proteins as detected by RNAseq during iPSC-differentiation in i^{3}Neurons (47). In contrast, the great majority of iPSC-derived DA neurons retained Arl13b-positive cilia (89.45 ± 1.68%; mean ± SEM), which were also positive for acetylated tubulin (a general cilia marker) and for adenylate cyclase type III (AC3), a marker specific of neuronal cilia (48, 49) (Fig. 2 *C–E*).

Cilia, as assessed by Arl13b, acetylated microtubules and AC3 immunolabeling, were almost twofold longer in SJ1 KO neurons when compared to control neurons, while the percentage of cilia-forming cells was the same in both conditions (Fig. 3 *A–F*). Furthermore, abnormally shaped Arl13b-positive cilia were observed in SJ1 KO DA neurons with the presence of misshaped or branched cilia in a small proportion of SJ1 KO DA neurons, but not in their controls (*SI Appendix*, Fig. S2 *A* and *B*). Interestingly, such morphological defects were not observed in control and SJ1 KO iPSCs (*SI Appendix*, Fig. S3 *A–C*), suggesting specific roles for SJ1 in neurons.

We next analyzed presence of cilia in two different iPSC-derived clones of SJ1^{RQ}KI DA neurons (Fig. 4). While again there was no difference in the percentage of cilia-forming DA neurons relative to controls, the length of cilia was significantly longer in both clones in comparison to control (Fig. 4 *A–E*). We conclude that lack of a functional SJ1 affects some properties of cilia in DA neurons.

Accumulation of $Ca_v1.3$ in Cilia of SJ1^{RQ}KI DA Neurons. A special property of DA neurons is an intrinsic pacemaker function, whose activity is highly dependent on the L-type $Ca_v1.2$ and $Ca_v1.3$ voltage-gated calcium channels (36–39). Interestingly, these channels, which are broadly localized throughout the surface of the cell bodies and dendrites of neurons (39) are also present in cilia or cilia-derived structures in several cell types, including cells of the retina and kidney (50–54). Prompted by this reported localization, we explored whether cilia of iPSC-derived DA neurons were labeled by anti-$Ca_v1.3$ antibodies that had been validated in $Ca_v1.3$ knockout cells (55). While we did not detect $Ca_v1.3$ immunoreactivity in the ciliary shaft of control iPSC-derived DA neurons, we found that $Ca_v1.3$ immunoreactivity displayed, as previously reported (50, 53), an accumulation at the base of their cilia, whose position was marked by γ-tubulin (Fig. 5 *A* and *B*). Strikingly, in SJ1^{RQ}KI DA neurons bright $Ca_v1.3$ fluorescence intensity was observed throughout the
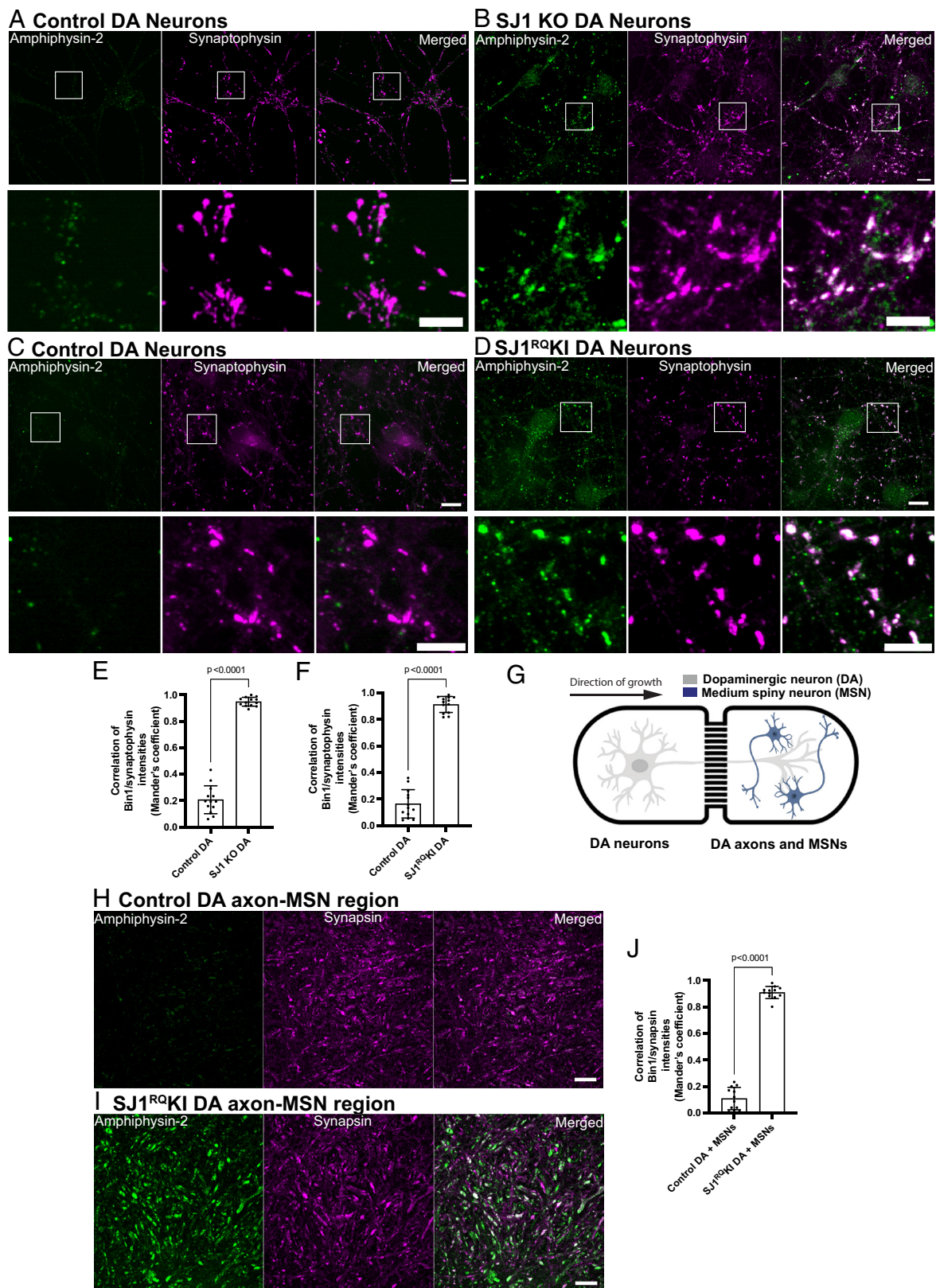
Fig. 1. SJ1 KO and SJ1^{RQ}KI iPSC-derived DA neurons show presynaptic clustering of amphiphysin-2. (*A–D*) Fluorescence images of control (*A* and *C*), SJ1 KO (*B*), and SJ1^{RQ}KI (*D*) DA neurons (days 50 to 55) immunolabeled with antibodies directed against amphiphysin-2 (green) and synaptophysin, a presynaptic marker, (magenta). SJ1 KO neurons and the corresponding controls are derived WTC11 iPSCs, while SJ1^{RQ}KI neurons and corresponding controls are derived from KOLF2.1 iPSCs (Scale bar, 10 μm). High magnifications of boxed areas are shown below each panel (Scale bar, 5 μm). Note the striking enhancement of amphiphysin-2 immunoreactivity that overlaps with synaptophysin-positive structures in SJ1 KO and SJ1^{RQ}KI DA neurons, relative to controls. (*E* and *F*) Quantification of amphiphysin-2 clustering intensities shown in (*A–D*), represented as mean ± SD, pooled from at least two independent experiments (n ≥ 10 cells per experiment). (*G*) Diagram showing a schematic view of iPSC-derived DA (day 55) and iPSC-derived MSNs (from Brainxell cells, day 7 post-thaw) cocultured in the microfluidic device. (*H* and *I*) Immunofluorescence images of amphiphysin-2 (green) and synapsin (magenta) immunoreactivities in the MSN containing chamber of neuronal cocultures generated with control (*H*) or SJ1^{RQ}KI DA neurons (*I*) (Scale bar, 10 μm). (*J*) Quantification of fluorescence intensity of amphiphysin-2 puncta in the MSN containing chamber (mean ± SD from two independent experiments; n ≥ 20 regions per experiment).
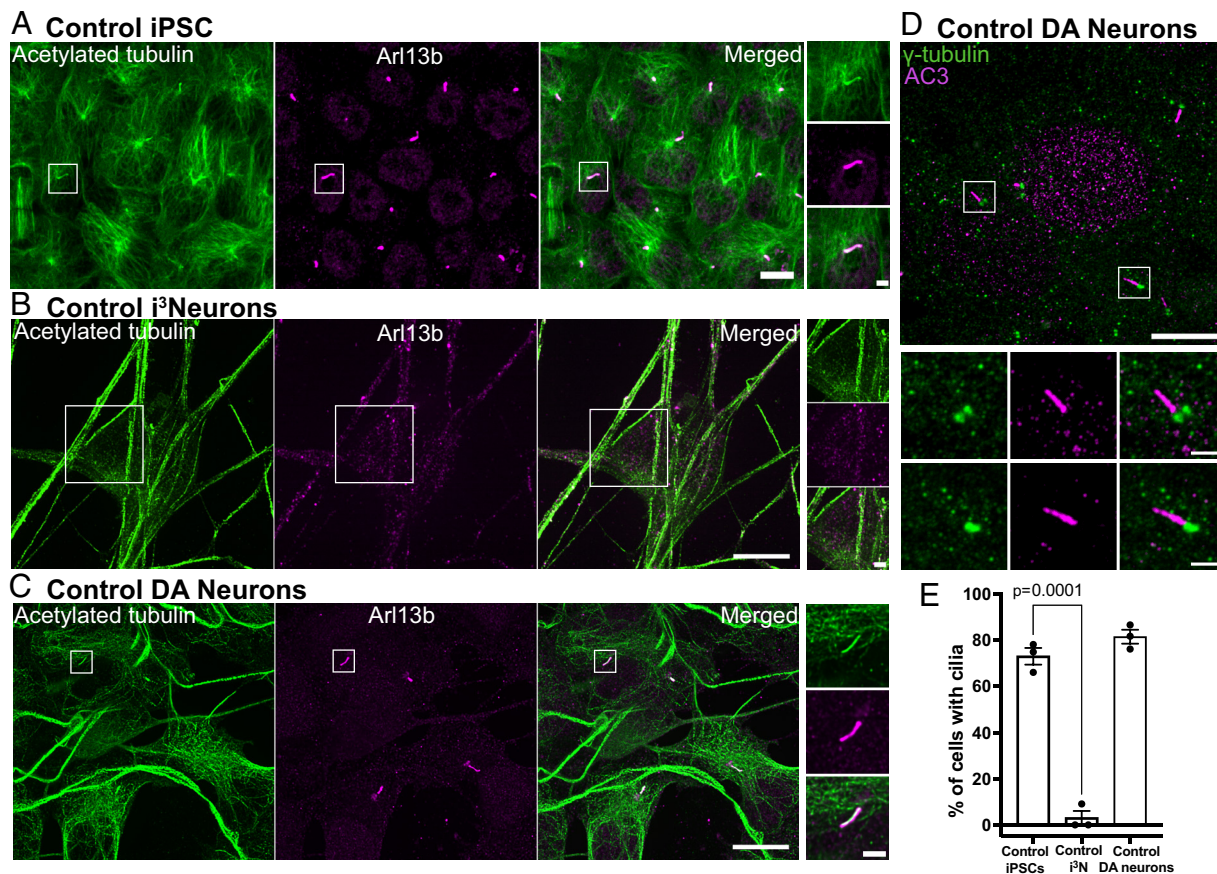
Fig. 2. iPSC-derived DA neurons have primary cilia. (*A–C*) Fluorescence images of undifferentiated iPSCs (*A*), i³Neurons (day 19, *B*), and iPSC-derived DA neurons (day 30, *D*) (all from KOLF2.1 iPSCs) immunolabeled with antibodies directed against acetylated α-tubulin (green) and Arl13b (magenta) (Scale bar, 10 μm). High-magnification images of the boxed areas in (*A–C*) are shown on the *Right* (Scale bar, 2 μm). iPSCs have primary cilia but cilia are no longer present in i³Neurons, while they are still present in DA neurons. (*D*) Fluorescence images of DA neurons immunolabeled with antibodies against γ-tubulin (green) and the neuronal-specific primary cilia marker, adenylate cyclase type III (AC3, magenta), confirming the neuronal properties of these neurons. (*E*) Percentage of cells with cilia (mean ± SEM) from three independent experiments; n ≥ 20 cells per experiment.

Arl13b-positive ciliary shaft (Fig. 5 *C–E*). It seems plausible that $Ca_v1.3$ may be present also in cilia, but not at a level detectable by immunofluorescence, and that the partial defect of SJ1 function due to the PD mutation results in its impaired clearance from cilia. These findings suggest that in iPSC-derived SJ1^{RQ}KI DA neurons, cilia are not only abnormal in length but also in some functional properties. Assessment of calcium signaling properties using the Fluo-4 dye showed reduced spontaneous activity in SJ1^{RQ}KI DA neurons when compared to control DA neurons (Fig. 5 *F–H*, Control: Movie S1; SJ1^{RQ}KI: Movie S2).

Accumulation of Ubiquitinated Proteins in SJ1^{RQ}KI DA Neurons. A major mechanism underlying turnover of membrane protein in cilia is their ubiquitination, primarily via lysine 63–linked Ub (UbK63) linkage, as this process controls their exit from cilia to allow their endocytosis and targeting for degradation (16, 56, 57). Thus, we investigated whether the presence of ubiquitin conjugates is higher in cilia using the well-characterized FK2 and FK1 monoclonal antibodies that label ubiquitin conjugates but not free ubiquitin (58) (Fig. 6). While no detectable FK2 and FK1 signal was observed in the cilia of control cells, a strong signal was present in cilia of SJ1^{RQ}KI DA neurons (Fig. 6 *A–F* and *SI Appendix,* Fig. S4A). This result reveals a link between SJ1 function and the clearance of proteins from cilia in DA neurons. Explanations for the clearing defect may include an impairment of the ciliary exit pathway or of endocytic traffic at the base of cilia.

Concentration of SJ1 at the Base of Primary Cilia. The impact of SJ1 mutations on primary cilia could be explained by the indirect effect of an endocytic impairment throughout the neuronal surface or to the loss of a specific function in proximity of cilia. To gain insight into this question, we assessed the localization of SJ1 by immunofluorescence in iPSCs before and after differentiation into DA neurons. We found that one or two closely apposed bright spots of SJ1 immunoreactivity colocalized with γ-tubulin, a marker of centrioles, were present in undifferentiated iPSCs and control DA neurons (Fig. 7 *A* and *B*). This staining at the base of cilia, was lost in SJ1 KO iPSCs and SJ1 KO DA neurons (Fig. 7 *C* and *D*). The localization of SJ1 at centrioles supports a role of SJ1 in cilia as it could serve as a mechanism to generate a focal high concentration of the protein in their proximity.

A frequently used model for the analysis of cilia is the RPE1 cell line, in which serum starvation for 48 h robustly induces ciliogenesis (Fig. 8*A*) (59, 60). Upon expression of either mCherry-SJ1-145 or GFP-tagged SJ1-170 (the short and long forms of SJ1, respectively, Fig. 8 *B* and *C*) in these cells, bright spots of mCherry and GFP fluorescence were observed at the base of primary cilia. Coexpression in these cells of mCherry-SJ1-145 with another phosphoinositide phosphatases, the 5-phosphatase INPP5E (GFP-INPP5E), a known component of the cilia shaft (20, 21) confirmed the specific and selective localization of SJ1 at the cilia base (Fig. 8*B*).
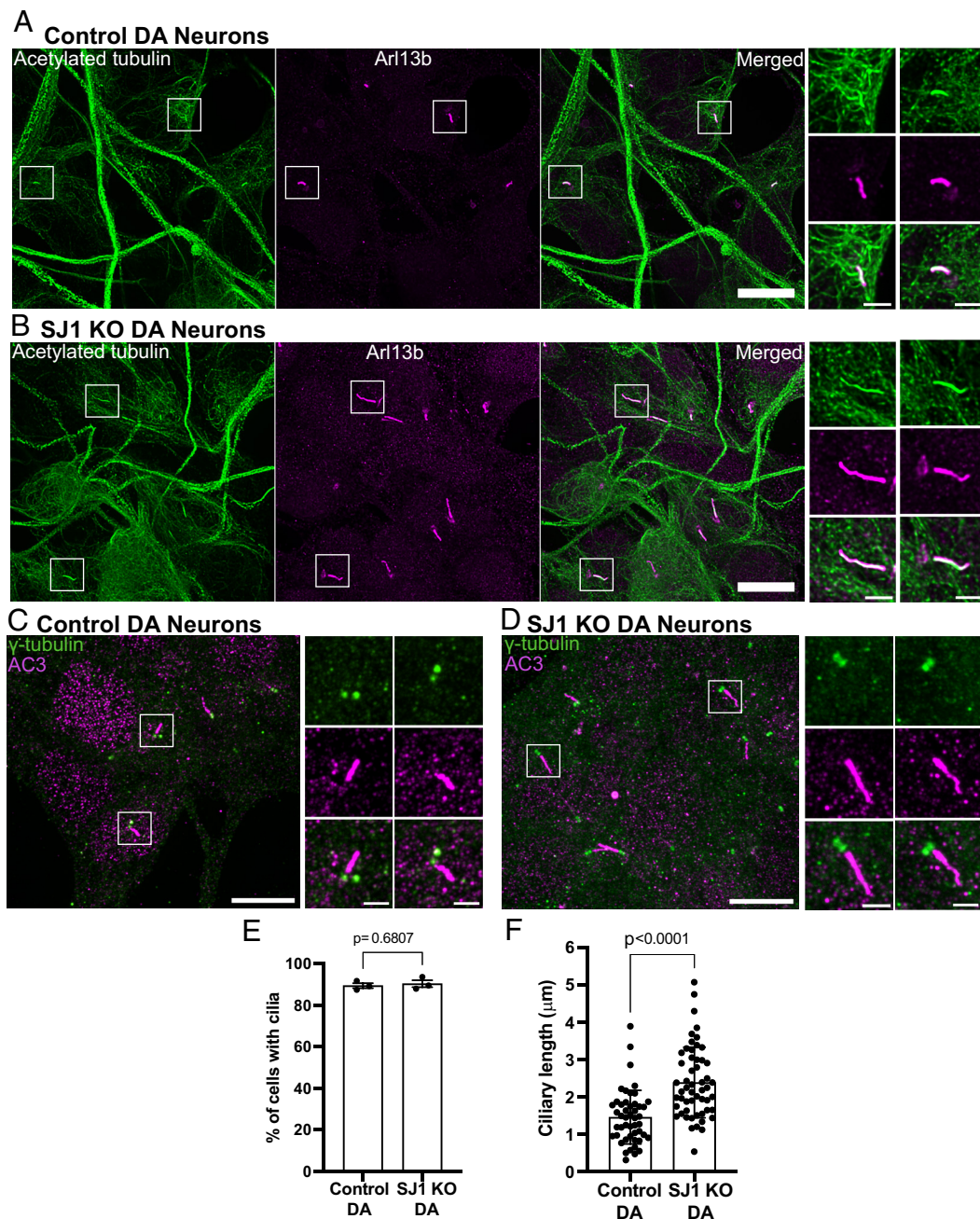
Fig. 3. Abnormal ciliary length in SJ1 KO iPSC-derived DA neurons relative to control iPSC-derived DA neurons. (*A–D*) Fluorescence images of control (*A* and *B*) and SJ1 KO (*C* and *D*) DA neurons (day 30) immunolabeled with antibodies against acetylated α-tubulin (green), Arl13b (magenta) or γ-tubulin (green) and the neuronal-specific primary cilia marker, AC3 (magenta) (Scale bar, 10 μm). High magnification of the boxed areas in (*A–D*) are shown on the *Right* of each panel (Scale bar, 2 μm). (*E* and *F*) Percentage of ciliated cells (*E*) and cilia length (*F*) of control and SJ1 KO DA neurons represented as mean ± SD (data pooled from three independent experiments; n ≥ 10 cells per experiment).

Discussion

Our study shows that impairment of SJ1 function in human iPSC-derived DA neurons has an impact on the properties of their primary cilia, in addition to the well-established disrupting effect on presynaptic vesicle traffic. Both the lack of SJ1 and the selective loss of its 4-phosphatase activity due to the EOP patient mutation (SJ1^{RQ}) lead to increased cilia length in these cells. Further analysis of cilia in SJ1^{RQ}KI iPSC-derived DA neurons revealed abnormal protein localization in them, as exemplified by the accumulation of the Ca$_v$1.3 channel and of ubiquitin chains throughout the ciliary shaft. Given the increasingly appreciated importance of primary cilia in neuronal signaling, it is plausible that a defect in

ciliary function may contribute to the pathological manifestations resulting from the EOP SJ1 mutation.

Traffic of plasma membrane proteins and lipids in and out of cilia is controlled by a diffusion barrier in which PI4P (which is the predominant phosphoinositide in the ciliary shaft) and PI(4, 5)P$_2$ (which is the predominant phosphoinositide in the ciliary pocket) play an important role (16–18, 61). Impairment of SJ1 function may disrupt the function of the diffusion barrier between the two compartments by perturbing the physiological concentration and relative ratio of PI4P and PI(4, 5)P$_2$. Alternatively, or in addition, SJ1 may help control membrane protein clearing from cilia indirectly via its function in the endocytic pathway (9) after the exit of these proteins from cilia
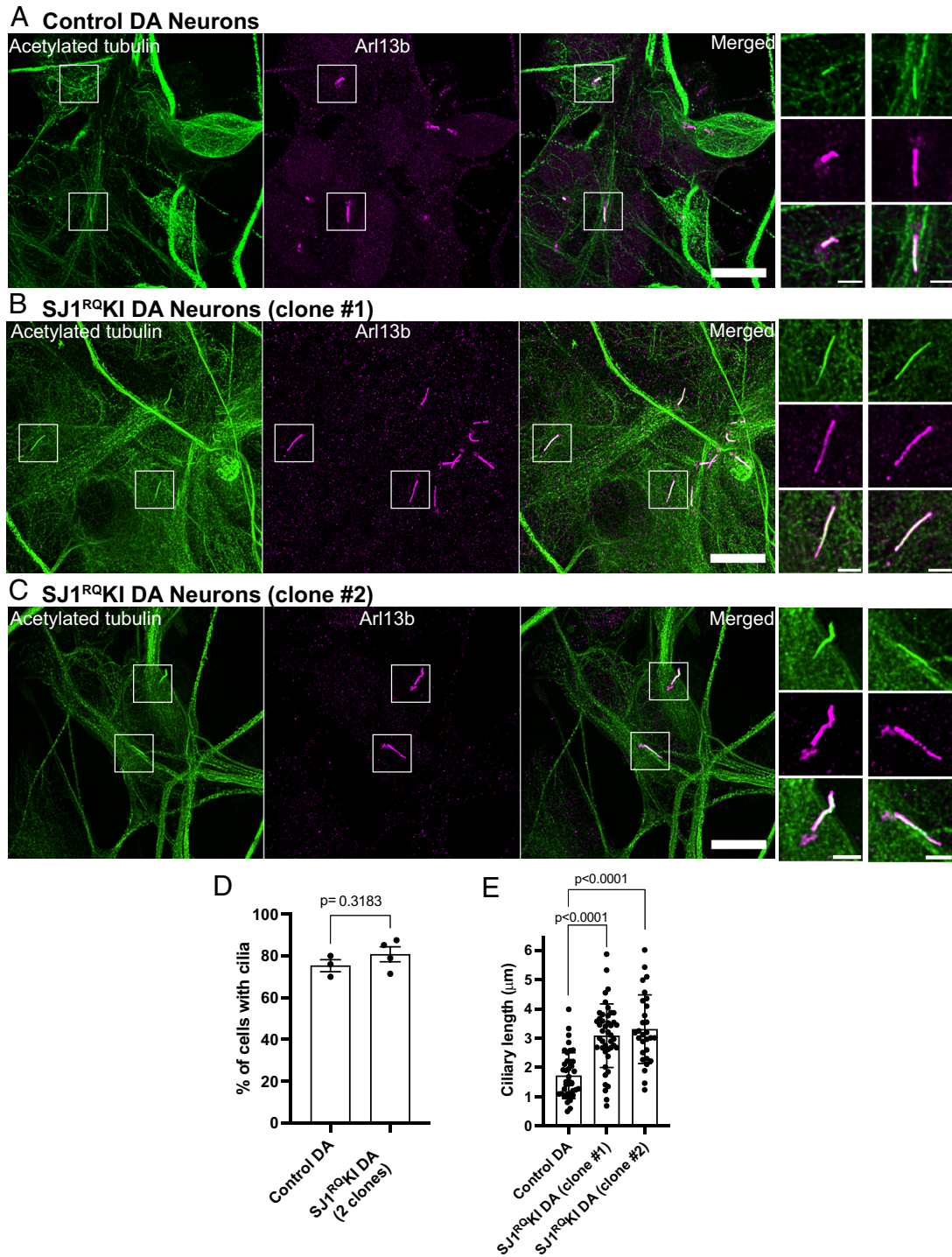
Fig. 4. Abnormal ciliary length also in iPSC-derived SJ1^{RQ}KI iPSC-derived DA neurons. (*A–D*) Fluorescence images of control (*A*) and SJ1^{RQ}KI (*B* and *C*) DA neurons (day 30) derived from two KOLF2.1 iPSC clones immunolabeled with antibodies directed against acetylated α-tubulin (green) and Arl13b (magenta) (Scale bar, 10 μm). High magnifications of the boxed areas in (*A–C*) are shown on the *Right* of each panel (Scale bar, 2 μm). (*D* and *E*) Percentage of ciliated cells (*D*) in control and SJ1^{RQ}KI DA neurons represented as mean ± SEM (from three independent experiments in which control neurons were grown in parallel with either mutant clone or both clones) (n ≥ 10 cells per experiment). (*E*) Ciliary length of the same control and SJ1^{RQ}KI DA neurons used for panel *D* represented (mean ± SD) n ≥ 10 cells per experiment.

(62, 63). While SJ1 appears to have a primary role in the shedding of endocytic factors after endocytosis (61), its loss-of-function, as shown by studies of nerve terminals, has shown to result in a backup of endocytic traffic with a partial stranding in the plasma membrane of proteins and membrane that needs to be internalized. As we have now shown that a pool of SJ1 is concentrated at the ciliary base, a special function of this protein in the overall ciliary membrane turnover due to endocytosis is still plausible.

Protein ubiquitination plays an important role in controlling protein turn-over in cilia, as a key regulatory mechanism for the exit of proteins from cilia is their ubiquitination (19, 56, 64). Thus, increased cilia length and abnormal accumulation of
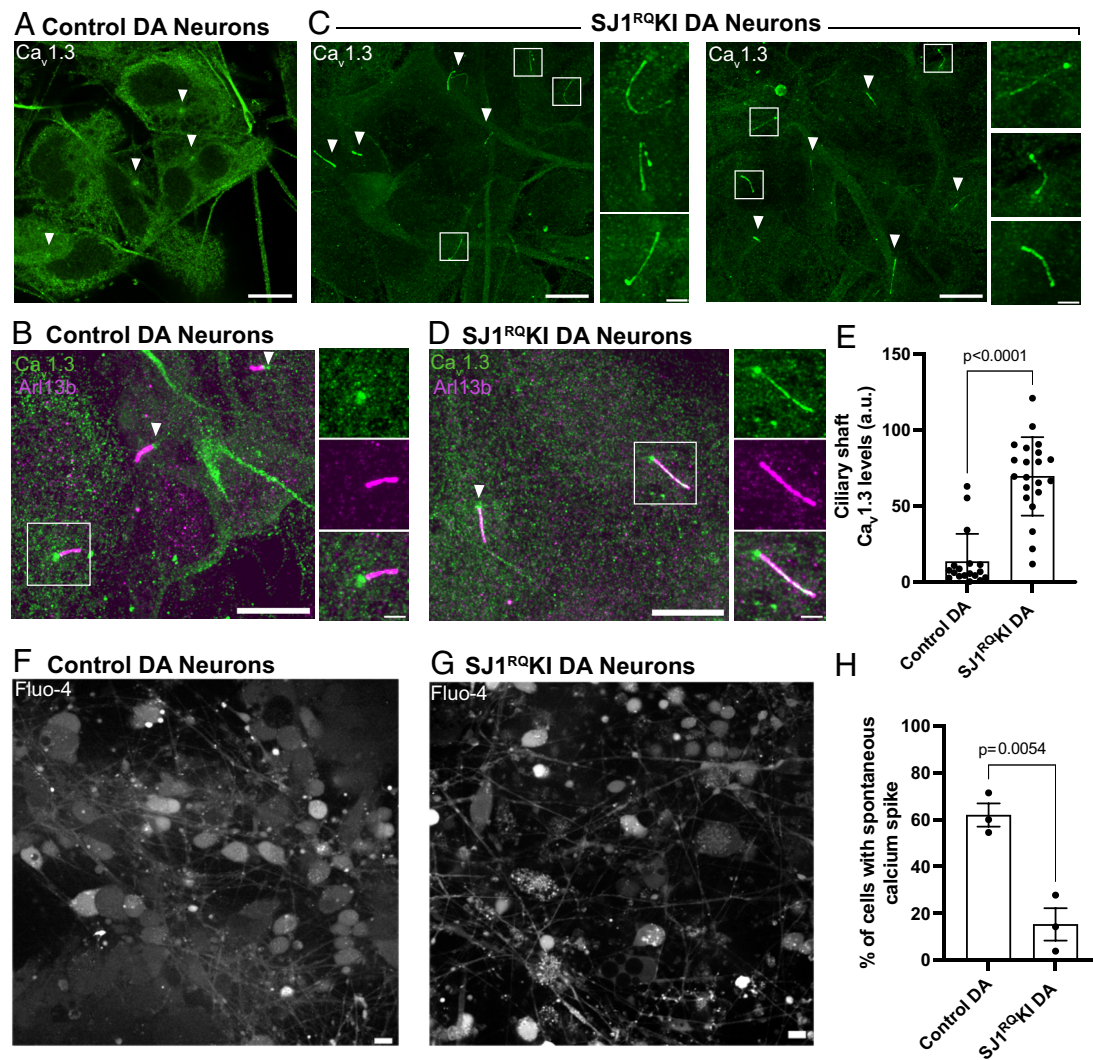
Fig. 5. Accumulation of $Ca_v1.3$ in the ciliary shaft of SJ1[RQ]KI iPSC-derived DA neurons. (*A* and *B*) Immunofluorescence images of control iPSC-derived DA neurons demonstrating that the shaft of cilia (labeled by Arl13b; magenta) is negative for Cav1.3, which only shows some accumulation at their base (arrowheads). (*C* and *D*) Immunofluorescence images of iPSC-derived SJ1[RQ]KI DA neurons demonstrating robust labeling for Cav1.3 (green) along the shaft of Arl13b-positive (magenta) cilia. (Scale bar, 10 µm; cropped areas: 2 µm). (*E*) Quantification of ciliary $Ca_v1.3$ immunoreactivity on the ciliary shaft of control and SJ1[RQ]KI DA neurons (mean ± SD pooled from three independent experiments; n ≥ 20 cells per experiment). (*F* and *G*) Fluorescence images of control (*F*, Movie S1) and SJ1[RQ]KI (*G*, Movie S2) DA neurons showing spontaneously occurring calcium spikes labeled with the calcium-binding dye, Fluo-4. (*H*) Percentage of DA neurons showing spontaneous calcium spikes in control (*F*) and SJ1[RQ]KI (*G*). Results reflect mean ± SEM pooled from three independent experiments (n ≥ 40 cells per experiment).

ubiquitinated proteins in cilia may be related and due to defective protein clearance from these cellular protrusions. The BBSome, a protein complex localized at cilia (65), is implicated in this clearance, and mutations in BBSome components perturb ciliary length (66–69). Interestingly, the BBSome components BBS7 and BBS9, as well as other proteins involved in centrosome/ciliary function, were hits in a proximity-labeling screen for SJ1 neighbors (70) suggesting a potential functional interplay between the BBsome and SJ1 in such clearing.

How SJ1 becomes concentrated at the base of cilia remain unclear. This localization is unlikely to be explained by its concentration on endocytic membranes in the ciliary pocket, since the localization of SJ1 closely overlaps with the localization of γ-tubulin even when the two centrioles are clearly physically separated, pointing to a concentration around the two centrioles rather than on endocytic vesicles. As the pericentriolar material is enriched in actin and actin regulatory proteins (62, 71–73), SJ1 may be recruited to these sites by interactions of its C-terminal proline-rich domain with actin-regulatory proteins (7). We suggest

that low affinity binding to proteins that surround the centrioles may serve to create a high local concentration of SJ1, thus facilitating its action at endocytic events that takes place at these sites. We note that another inositol 5-phosphatase implicated in endocytic traffic was shown to be concentrated on centrioles at the base of cilia and impact cilia length, although with conflicting results about cilia length (74–76), with longer cilia in Rbaibi et al. (75).

A role in primary cilia dynamics in PD pathogenesis has been previously suggested (24, 26, 77). In particular, at least some effects of the PD gene LRRK2 have been attributed to a role of this protein in cilia, based on studies in cell lines and mouse brain tissue (26, 32, 35). PD mutations in LRRK2 resulted in shorter rather than longer cilia as we have shown here for SJ1 mutations. However, it remains possible that some shared aspects of ciliary function may be disrupted by both PD LRRK2 mutations and the EOP SJ1 mutation, in spite of the different effect on cilia morphology. Moreover, studies of LRRK2 and cilia have focused on striatal cells, i.e., targets of dopaminergic innervation, while here we have focused on DA
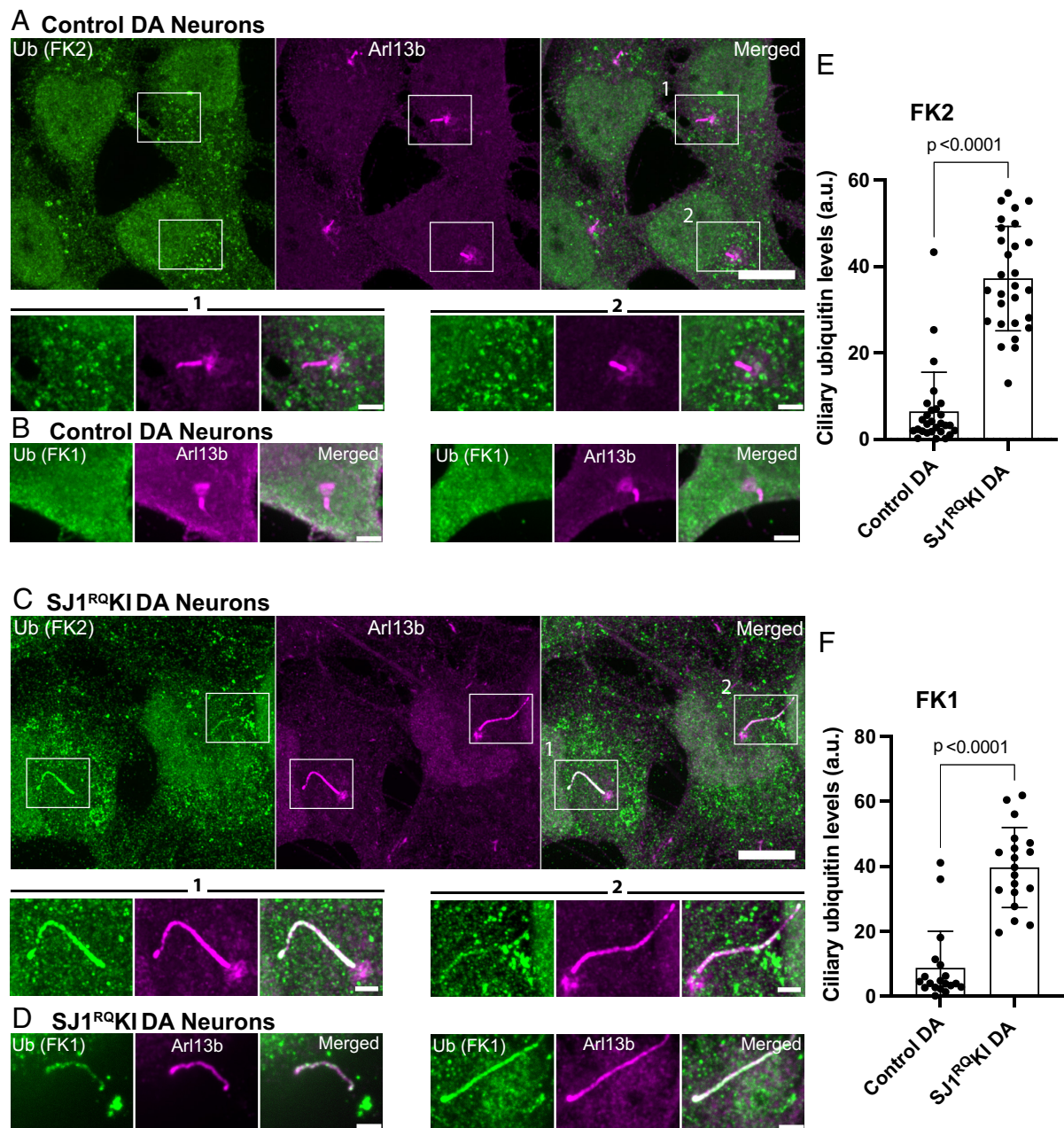
Fig. 6. Accumulation of ubiquitin conjugates in cilia of iPSC-derived SJ1[RQ]KI DA neurons. (*A–C*) Fluorescence images of control (*A* and *B*) and SJ1[RQ]KI (*C* and *D*) DA neurons (day 30) immunolabeled with antibodies directed against lysine 63-linked ubiquitin chains (FK2 or FK1 antibodies, as indicated) (green) and Arl13b (magenta) (Scale bar, 10 μm). For FK2, both low and high magnifications of the boxed areas are shown (Scale bar, 2 μm) while for FK1, only high magnifications are shown. (*E* and *F*) Quantification of FK2 and FK1 immunoreactivities in the ciliary shaft of control and SJ1[RQ]KI DA neurons. Results for FK2 reflect mean ± SD pooled from four independent experiments (n ≥ 15 cells per experiment). Results for FK1 reflect mean ± SD pooled from three independent experiments (n ≥ 15 cells per experiment).

neurons. An additional role of LRRK2 mutations on cilia of DA neurons cannot be excluded.

Whether and how the abnormal features of cilia of SJ1 mutant DA neurons impact their function will require further investigations. Ca^{2+} oscillations in primary cilia independent of somatic Ca^{2+} levels have been detected in several cell types and attributed to ciliary calcium channel activation, suggesting that cilia could function as an autonomous Ca^{2+} signaling hub in response to external stimuli (54, 78–80). In this context, the striking accumulation of $Ca_v1.3$ proteins in the cilia of SJ1[RQ]KI DA neurons is of special interest as it raises the possibility that Ca^{2+} signaling in these cilia may be altered, with repercussion on cell physiology.

SJ1 KO mice, which die perinatally, do not display obvious brain developmental defects at birth. Likewise, developmental defects are not observed in mice and humans with the EOP mutation. Thus, the impact of SJ1 on cilia function must be more subtle than the one of other proteins whose mutations results in major such defects, collectively referred to as ciliopathies (81). Similar considerations were made for LRRK2 mutations (26) and OCRL mutation (75).

In conclusion, our study reveals a role of SJ1 in primary cilia of DA neurons and raises the possibility that perturbation of such a role by the EOP mutation may contribute to the pathological manifestations produced by this mutation.
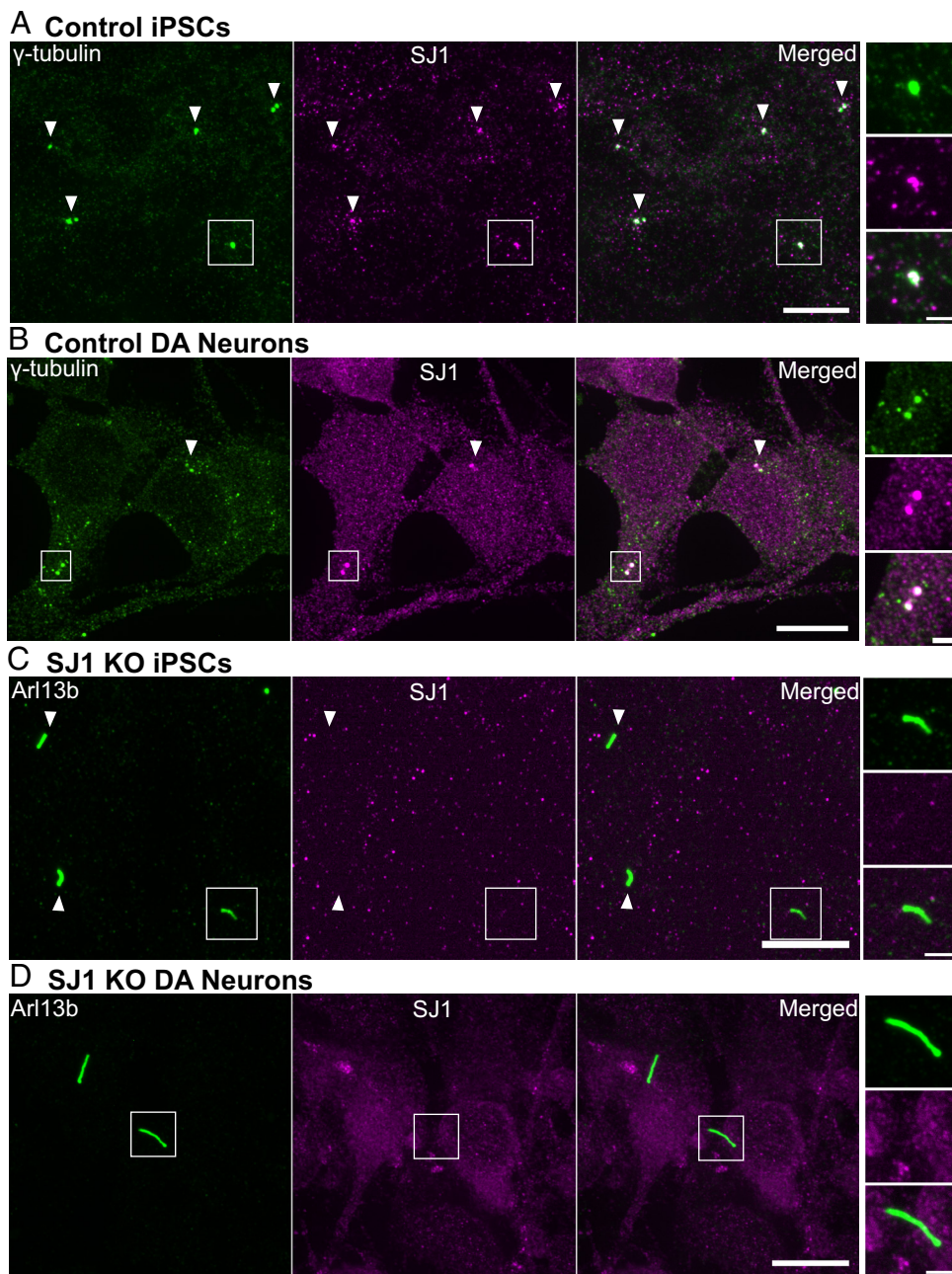
Fig. 7. Presence of a pool of SJ1 at the ciliary base of iPSCs and iPSC-derived DA neurons. (*A* and *B*) Fluorescence images of control (*A*) iPSCs and (*B*) iPSC-derived DA neurons immunolabeled with antibodies directed against γ-tubulin (green) and SJ1 (magenta) showing overlap of spots of SJ1 immunoreactivity in control but not in SJ1 KO cells. (*C* and *D*) Fluorescence image of SJ1 KO iPSCs and iPSC-derived SJ1 KO DA neurons (day 30) immunolabeled with antibodies against Arl13b (green) and SJ1 (magenta) showing lack of SJ1 staining at the base of cilia. High magnifications of boxed areas in (*A–D*) are shown at *Right*. (Scale bar, 10 μm; cropped areas: 2 μm).

Materials and Method

Antibodies and Plasmids. mCherry-synaptojanin-145 (neuronal isoform, UniProt entry: O43426-2), GFP-synaptojanin-1-170 (non-neuronal isoform, UniProt entry: O43426), and GFP-INPP5E were previously generated in the De Camilli lab. Each construct was validated by DNA sequencing. All antibodies used in this study are listed in *SI Appendix*, Table S1.

Human iPSC Culture, i³Neuron, and DA Differentiation. The following iPSC lines were obtained from the iNDI consortium and genome-edited by Jackson Laboratories (JAX): KOLF2.1, KOLF2.1 (with the NGN2 cassette at the AAVS locus; RRID:CVCL_D1KS), used for the i³Neurons experiments) and KOLF2.1 SJ1^RQ KI (R219Q): clones A09 and B02. The WTC11 (with the NGN2 cassette at the AAVS locus) iPSC line, kind gift of M. Ward (NIH, Bethesda, MD) was used to generate SJ1 KO cells. For the maintenance of iPSCs in culture, iPSCs were cultured on Geltrex (Life Technologies) coated dishes and maintained in Essential 8 Flex media (Thermo Fisher Scientific). The Rho-kinase (ROCK) inhibitor Y-27632 (EMD Millipore, 10 μM) was added to Essential 8 Flex media on

the first day of plating and replaced with fresh media without ROCK inhibitor on the following day.

For i³neuronal differentiation, iPSCs were differentiated into cortical-like i³Neurons according to a previously described protocol based on the doxycycline inducible expression of Ngn2 (42). Briefly, iPSCs were dissociated with Accutase (Thermo Fisher Scientific) and replated at a density between 1.5 and 3 × 10⁵ cells on geltrex-coated dishes in induction medium [(KnockOut DMEM/F-12 (Thermo Fisher Scientific) containing 1% N2-supplement (Thermo Fisher Scientific), 1% MEM nonessential amino acids (Thermo Fisher Scientific), 1% GlutaMAX (Thermo Fisher Scientific), and 4 μg/mL doxycycline (Sigma-Aldrich)]. After 3 d, prediffer-entiated i³Neurons were dispersed using Accutase and plated on 0.1 mg/mL poly-L-ornithine (Sigma-Aldrich) in borate buffer and 10 μg/mL laminin (Thermo Fisher Scientific) coated 35 mm glass-bottom dishes (MatTek) or 6-well plates (Corning) for imaging and immunoblotting, respectively. These i³Neurons were cultured and maintained in cortical medium (induction medium supplemented with 2% B27 (Thermo Fisher Scientific), 10 ng/mL BDNF (PeproTech), 10 ng/mL NT-3 (PeproTech), and 10 μg/mL laminin). Fresh cortical media were added to
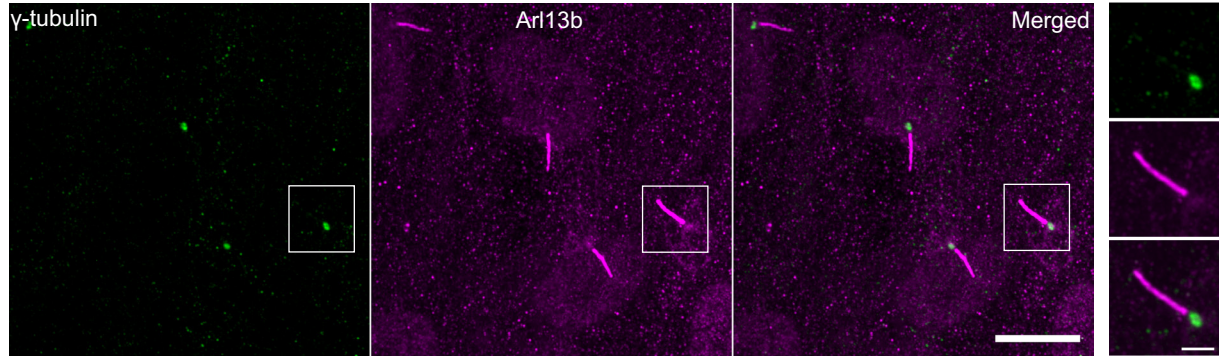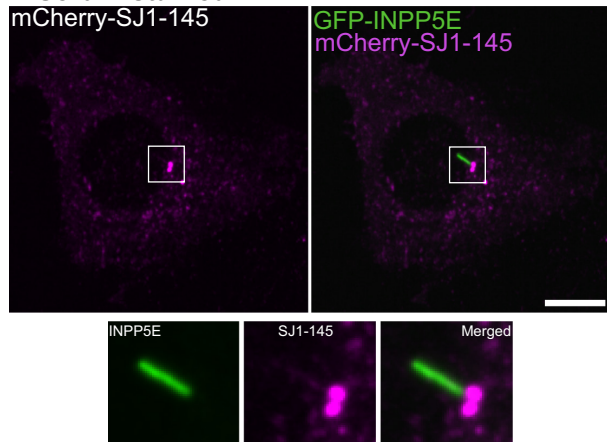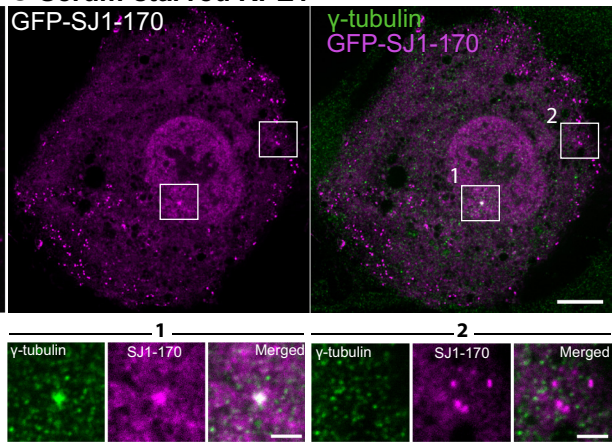
Fig. 8. Exogenously expressed tagged-SJ1 labels the base of cilia. (*A*) Fluorescence image of RPE1 serum-starved for 48 h and immunolabeled with antibodies against γ-tubulin (green) and Arl13b (magenta) show primary cilia assemblies. (*B*) Live fluorescence image of serum-starved RPE1 cell expressing mCherry-SJ1-145 (neuronal isoform, magenta) and GFP-INPP5E (green, a ciliary marker) showing localization of SJ1 at the ciliary base. The boxed area is shown at high magnification below the main figure. (*C*) Fluorescence image of serum-starved RPE1 expressing GFP-SJ1-170 (non-neuronal isoform, magenta) and immunolabeled with antibodies against γ-tubulin (green) showing overlap of the two proteins on a single perinuclear spot (boxed area 1). Boxed area 2 shows that while puncta of GFP-SJ1-170 are also observed elsewhere in the cell, these puncta do not overlap with γ-tubulin. (Scale bar, 10 μm; cropped areas: 2 μm).

the existing media every 5 d. The iPSCs and i³Neurons were kept at 37 °C with 5% CO2 in an enclosed incubator. A detailed protocol can be found at https://www.protocols.io/view/culturing-i3neurons-basic-protocol-6-n92ld3kbng5b/v1.

For the differentiation of iPSCs to DA neurons, we used the following protocols described in Kriks et al. (28) and Bressan, Dhingra, Donato, and Heutink (43). Briefly, iPSCs were dissociated with Accutase (Thermo Fisher Scientific) and replated at a density of 8×10^5 cells per well (of a 6-well plate) on geltrex-coated dishes in Essential 8 Flex media with Rock inhibitor. On the next day (Day 0 of differentiation), the media was replaced with knockout serum replacement (KSR) media containing 500 nM LDN193189 (STEMCELL Technologies) and 10 μM SB431542 (STEMCELL Technologies). KSR medium is composed of Knockout DMEM/F12 medium, 15% Knockout serum replacement (Thermo Fisher Scientific), 1% MEM NEAA, 1% glutaMAX, 0.1% 2-mercaptopethanol (Thermo Fisher Scientific) and 0.2% penicillin-streptomycin (Thermo Fisher Scientific). Starting the following day (day 1) 75% of the differentiation medium was replaced with a new medium each day from day 1 to day 15, then every 2 d until day 20. For days 1 to 4, KSR medium containing 500 nM LDN193189, 10 μM SB431542, 200 ng/mL SHH C25II (R&D Systems), 2 μM Purmorphamine (Cayman Chemical Company), and 100 ng/mL FGF-8b (PeproTech) was added daily, supplemented by the addition of 4 μM CHIR99021 on days 3 and 4. For days 5 and 6, a mixture of 75% KSR + 25% N2 medium also containing 500 nM LDN193189, 10 μM SB431542, 200 ng/mL SHH C25II (R&D Systems), 2 μM Purmorphamine (Cayman Chemical Company), 100 ng/mL FGF-8b (PeproTech), and 4 μM CHIR99021 (Tocris) was added to the cells followed by equal amounts of KSR and N2 media on days 7 to 8, and 25% KSR + 75% N2 media on days 9 to 10 also containing 500 nM LDN193189, 10 μM SB431542, 200 ng/mL SHH C25II, and 4 μM CHIR99021. The N2 medium is composed of Neurobasal Plus media (Thermo Fisher Scientific), 2% B27 supplement without vitamin A (Thermo Fisher

Scientific), 1% N2 supplement, 1% glutaMAX, and 0.2% penicillin-streptomycin. For days 11 to 20, complete NB/B27 medium was added to cells, with the addition of 4 μM CHIR99021 on days 11 and 12 only. Complete NB/B27 medium is composed of N2 medium (without the N2 supplement) and the following components: 20 ng/mL BDNF (PeproTech), 0.2 mM ascorbic acid (Sigma-Aldrich), 20 ng/mL GDNF (PeproTech), 0.5 mM db-cAMP (Sigma-Aldrich), 1 ng/mL TGFβ3 (R&D Systems), and 10 μM DAPT (Cayman Chemical Company). After 20 d of culture, DA progenitors cells were frozen in Synth-a-freeze cryopreservation media (Thermo Fisher Scientific) and stored at −80 °C or liquid nitrogen.

For long-term culture of DA neurons, cells were replated on 0.1 mg/mL poly-L-ornithine in PBS (Sigma-Aldrich) and 10 μg/mL laminin (Thermo Fisher Scientific) coated 35 mm glass-bottom dishes (MatTek) or 6-well plates (Corning) for imaging and immunoblotting, respectively. These neurons were cultured and maintained in complete NB/B27 medium followed by the addition of 0.1% antimitotic inhibitor (Supplement K, Brainxell) at day 25 to terminate division of non-neuronal cells. Fresh NB/B27 medium was added to the existing plates or dishes every 7 d and kept at 37 °C with 5% CO2 in an enclosed incubator. A detailed protocol can be found at 10.17504/protocols.io.dm6gp39m8vzp/v1.

CRISPR–Cas9 Mediated Generation of SJ1 KO iPSCs. A CRISPR-based homologous recombination strategy was used to generate the SJ1 KO iPSC line. Briefly, 1×10^5 WTC11-NGN2 iPSCs were plated on Geltrex-coated 6-well plate and transfected the following day using the Lipofectamine Stem transfection reagent (Invitrogen) and 3 μg of px458 plasmid (RRID:Addgene_ 48138) containing a small guide RNA with the following sense (5′C CACCGTGGTTATTACGTCTTATGTG3′) and antisense (5′AAACCACATAAGACGTAATAACCAC3′) sequences that was designed to selectively target the Exon 5 of SJ1. Pooled (GFP-positive) cells were enriched by fluorescence activated cell sorting (FACS) 2 d later. Sorted cells were expanded

and then serially diluted to yield small clonal populations, screened using PCR amplification of genomic DNA flanking the sgRNA target site followed by sequencing of the amplicons using the following forward and reverse sequencing primers: 5′TCTCGTTTTATAGCCCTATCTTCTGATCC3′, 5′AAGGCCCATAAGTAACCAAGAA CAATC3′, respectively. A detailed protocol can be found at 10.17504/protocols. io.36wgqnr33gk5/v1.

Cell Culture and Transfections. hTERT-RPE1 cells (RRID: CVCL_4388) were grown in DMEM/F12 (Thermo Fisher Scientific) supplemented with 10% FBS (Thermo Fisher Scientific), 1% glutaMAX and 1% penicillin-streptomycin. Cells were kept at 37 °C with 5% CO2 in an enclosed incubator. Cells were transfected with the relevant plasmids using 4 μL of Lipofectamine™ 2000 Transfection Reagent (Invitrogen). Four to six hours post-transfection the medium was changed to DMEM/F12 medium without FBS to induce ciliogenesis and examined at the microscope 48 h later. For both i3Neuron and DA neuron transfections, plasmids were transfected with 4 μL of Lipofectamine™ Stem Transfection Reagent (Invitrogen) and visualized at least 48 h later. A detailed protocol can be found at 10.17504/protocols.io.5qpvokx3bl4o/v1.

Immunofluorescence, Live Imaging, and Fluorescent Microscopy. Cells were seeded on glass-bottom mat-tek dishes (MATtek corporation). For immunofluorescence, cells were fixed with 4% (v/v) paraformaldehyde (Electron Microscopy Sciences) in 1x phosphate-buffered saline (PBS) for 20 min followed by three washes in PBS. Cells were permeabilized with 0.25 to 0.5% (v/v) Triton X-100 in PBS for 5 min followed by three washes in PBS. Cells were then incubated with fresh 1 mg/mL sodium borohydride (Sigma-Aldrich) in PBS for 7 min to reduce autofluorescence and then washed thrice in PBS. They were further blocked for 30 min in 5% bovine serum albumin (BSA, Sigma-Aldrich) in PBS and then incubated overnight at 4 °C with the primary antibodies listed in *SI Appendix*, Table S1. Subsequently, cells were washed with PBS thrice the following day and incubated with Alexa Fluor-conjugated secondary antibodies (Thermo Fisher Scientific) for 1 h at room temperature, followed by three washes in PBS. DAPI (Thermo Fisher Scientific) was used for nuclear staining.

For calcium imaging, cells were incubated with FLUO-4 (Thermo Fisher Scientific) at a final concentration of 1 μM for 15 min followed by 2 washes in neuronal media.

Transfections were carried out as described above. For live imaging, cells were maintained in Live Cell Imaging buffer (Life Technologies) for COS7 cells, while both i3Neurons and DA neurons were maintained in CM and NB/B27 media, respectively, in a caged incubator with humidified atmosphere (5% CO$_2$) at 37 °C. The Yokogawa spinning disk field scanning confocal system with microlensing (CSU-W1 SoRa, Nikon) controlled by NIS elements (Nikon) software (RRID:SCR_014329) was used for neuronal imaging. Excitation wavelengths between 405 and 640 nm, CFI SR Plan ApoIR 60XC WI objective lens, and SoRa lens-switched light path at 1×, 2.8×, or 4× were used. SoRa images were deconvolved using the Batch Deconvolution (Nikon) software. A detailed protocol can be found at 10.17504/protocols.io.5qpvokx3bl4o/v1.

Neuronal Coculture Device. Control or SJ1RQKI DA neurons (day 30) were replated on one side of the two-chamber microfluidic compartmentalization device (OMEGA4, eNuvio), where only axonal processes can migrate through the microfluidic channels connected to the adjacent chamber. After an additional 25 d in the coculture device, frozen iPSC-derived MSNs from Brainxell were plated on the other half of the device (where only the axons of DA neurons are present). The DA-MSN cocultures were then fixed 7 to 10 d later for immunofluorescence. A detailed protocol can be found at 10.17504/protocols.io.dm6gpze38lzp/v1.

Immunoblotting. i3Neurons, DA neurons, and MSNs were grown on six-well plates (3 to 5 × 10^5 cells/well). After differentiation in their respective maturation media, neurons were washed with ice-cold PBS and then lysed in 1xRIPA lysis buffer (10× RIPA lysis buffer, Sigma-Aldrich) supplemented with cOmplete™ EDTA-free protease inhibitor cocktail (Roche) and PhosSTOP phosphatase inhibitor cocktail (Roche), followed by centrifugation at 13,000 × g for 6 min. The supernatant was collected and incubated at 95 °C for 5 min in SDS sample buffer containing 1% 2-mercaptoethanol (Sigma). The extracted proteins were separated by SDS-PAGE in Mini-PROTEAN TGX precast polyacrylamide gels (Bio-Rad) and transferred to nitrocellulose membranes (Bio-Rad) at 100 V for 1 h or 75 V for 2 h (for high molecular weight proteins: >150 kDa). Subsequently, the nitrocellulose membranes were blocked for 1 h with 5% nonfat milk (AmericanBIO) in TBST (tris-buffered saline [TBS] + 0.1% tween 20), then incubated overnight at 4 °C with primary antibodies and then incubated with IRDye 680RD or 800CW (LI-COR) secondary antibodies (1:8,000) (RRID:AB_2716687; RRID:AB_2651128; RRID:AB_2814912; RRID:AB_10953628; RRID:AB_10956166; RRID:AB_10956590) for 1 h at room temperature in TBST. Finally, blots were imaged using the Gel Doc imaging system (Bio-Rad) using the manufacturer's protocols. A detailed protocol can be found at 10.17504/protocols.io.3byl49eqjgo5/v1.

Statistical Analysis. Quantification of ciliary ubiquitination and Ca$_v$1.3 levels were carried out according to Shinde, Nager, and Nachury (56). Briefly, total fluorescence intensity of ubiquitin or Ca$_v$1.3 levels at individual Arl13b-positive cilium were subtracted from background ubiquitin or Ca$_v$1.3 fluorescence measured in the adjacent area. The methods for statistical analysis and sizes of the samples (n) are specified in the results section or figure legends for all quantitative data. Student's *t* test or Mann–Whitney test was used when comparing two datasets. Differences were accepted as significant for $P < 0.05$. Prism version 9 (GraphPad Software) (RRID:SCR_002798) was used to plot, analyze, and represent the data.

1. C. Blauwendraat, M. A. Nalls, A. B. Singleton, The genetic architecture of Parkinson's disease. *Lancet Neurol.* **19**, 170–178 (2020).
2. P. S. McPherson *et al.*, A presynaptic inositol-5-phosphatase. *Nature* **379**, 353–357 (1996).
3. C. E. Krebs *et al.*, The Sac1 domain of SYNJ1 identified mutated in a family with early-onset progressive Parkinsonism with generalized seizures. *Hum. Mutat.* **34**, 1200–1207 (2013).
4. M. Quadri *et al.*, Mutation in the SYNJ1 gene associated with autosomal recessive, early-onset Parkinsonism. *Hum. Mutat.* **34**, 1208–1215 (2013).
5. S. Guo, L. E. Stolz, S. M. Lemrow, J. D. York, SAC1-like domains of yeast SAC1, INP52, and INP53 and of human synaptojanin encode polyphosphoinositide phosphatases. *J. Biol. Chem.* **274**, 12990–12995 (1999).
6. Y. Nemoto *et al.*, Functional characterization of a mammalian Sac1 and mutants exhibiting substrate-specific defects in phosphoinositide phosphatase activity. *J. Biol. Chem.* **275**, 34293–34305 (2000).
7. E. Rosivatz, Interactions of synaptojanin. *Signal Transduction* **6**, 101–111 (2006).
8. A. R. Ramjaun, P. S. McPherson, Tissue-specific alternative splicing generates two synaptojanin isoforms with differential membrane binding properties. *J. Biol. Chem.* **271**, 24856–24861 (1996).
9. O. Cremona *et al.*, Essential role of phosphoinositide metabolism in synaptic vesicle recycling. *Cell* **99**, 179–188 (1999).
10. G. Di Paolo, P. De Camilli, Phosphoinositides in cell regulation and membrane dynamics. *Nature* **443**, 651–657 (2006).
11. D. A. Dyment *et al.*, Homozygous nonsense mutation in SYNJ1 associated with intractable epilepsy and tau pathology. *Neurobiol. Aging* **36**, 1222.e1–1222.e5 (2015).
12. K. Hardies *et al.*, Loss of SYNJ1 dual phosphatase activity leads to early onset refractory seizures and progressive neurological decline. *Brain* **139**, 2420–2430 (2016).
13. M. Cao *et al.*, Parkinson Sac domain mutation in synaptojanin 1 impairs clathrin uncoating at synapses and triggers dystrophic changes in dopaminergic axons. *Neuron* **93**, 882–896.e5 (2017).
14. X. Y. Ng *et al.*, Mutations in Parkinsonism-linked endocytic proteins synaptojanin1 and auxilin have synergistic effects on dopaminergic axonal pathology. *NPJ Parkinsons Dis.* **9**, 26 (2023).
15. L. Demmel *et al.*, The endocytic activity of the flagellar pocket in Trypanosoma brucei is regulated by an adjacent phosphatidylinositol phosphate kinase. *J. Cell Sci.* **129**, 2285 (2016).
16. I. Ojeda Naharros, M. V. Nachury, Shedding of ciliary vesicles at a glance. *J. Cell Sci.* **135**, jcs246553 (2022).
17. F. R. Garcia-Gonzalo *et al.*, Phosphoinositides regulate ciliary protein trafficking to modulate hedgehog signaling. *Dev. Cell* **34**, 400–409 (2015).
18. M. Chavez *et al.*, Modulation of ciliary phosphoinositide content regulates trafficking and Sonic hedgehog signaling output. *Dev. Cell* **34**, 338–350 (2015).
19. M. V. Nachury, D. U. Mick, Establishing and regulating the composition of cilia for signal transduction. *Nat. Rev. Mol. Cell Biol.* **20**, 389–405 (2019).
20. S. L. Bielas *et al.*, Mutations in INPP5E, encoding inositol polyphosphate-5-phosphatase E, link phosphatidyl inositol signaling to the ciliopathies. *Nat. Genet.* **41**, 1032–1036 (2009).
21. M. Jacoby *et al.*, INPP5E mutations cause primary cilium signaling defects, ciliary instability and ciliopathies in human and mouse. *Nat. Genet.* **41**, 1027–1031 (2009).
22. S. C. Phua *et al.*, Dynamic remodeling of membrane composition drives cell cycle through primary cilia excision. *Cell* **168**, 264–279.e15 (2017).
23. B. U. Klink, C. Gatsogiannis, O. Hofnagel, A. Wittinghofer, S. Raunser, Structure of the human BBSome core complex. *Elife* **9**, e53910 (2020).
24. U. Nordstroma *et al.*, Progressive nigrostriatal terminal dysfunction and degeneration in the engrailed1 heterozygous mouse model of Parkinson's disease. *Neurobiol. Dis.* **73**, 70–82 (2015).

25. M. Hynes et al., Induction of midbrain dopaminergic neurons by Sonic hedgehog. *Neuron* **15**, 35–44 (1995).
26. H. S. Dhekne et al., A pathway for Parkinson's disease LRRK2 kinase to block primary cilia and Sonic hedgehog signaling in the brain. *Elife* **7**, e40202 (2018).
27. C. Derderian, G. I. Canales, J. F. Reiter, Seriously cilia: A tiny organelle illuminates evolution, disease, and intercellular communication. *Dev. Cell* **58**, 1333–1349 (2023).
28. S. Kriks et al., Dopamine neurons derived from human ES cells efficiently engraft in animal models of Parkinson's disease. *Nature* **480**, 547–551 (2011).
29. T. W. Kim et al., Biphasic activation of WNT signaling facilitates the derivation of midbrain dopamine neurons from hESCs for translational use. *Cell Stem Cell* **28**, 343–355.e5 (2021).
30. D. R. Alessi, E. Sammler, LRRK2 kinase in Parkinson's disease. *Science* **360**, 36–37 (2018).
31. W. Poewe et al., Parkinson disease. *Nat. Rev. Dis. Primers* **3**, 17013 (2017).
32. Y. Sobu, P. S. Wawro, H. S. Dhekne, W. M. Yeshaw, S. R. Pfeffer, Pathogenic LRRK2 regulates ciliation probability upstream of tau tubulin kinase 2 via Rab10 and RILPL1 proteins. *Proc. Natl. Acad. Sci. U.S.A.* **118**, e2005894118 (2021).
33. C. Paisan-Ruiz et al., Cloning of the gene containing mutations that cause PARK8-linked Parkinson's disease. *Neuron* **44**, 595–600 (2004).
34. A. Zimprich et al., Mutations in LRRK2 cause autosomal-dominant parkinsonism with pleomorphic pathology. *Neuron* **44**, 601–607 (2004).
35. S. S. Khan et al., Pathogenic LRRK2 control of primary cilia and Hedgehog signaling in neurons and astrocytes of mouse brain. *Elife* **10**, e67900 (2021).
36. R. Felix, N. Weiss, Ubiquitination and proteasome-mediated degradation of voltage-gated Ca2+ channels and potential pathophysiological implications. *Gen. Physiol. Biophys.* **36**, 1–5 (2017).
37. L. Grimaldo, A. Sandoval, P. Duran, L. Gomez Flores-Ramos, R. Felix, The ubiquitin E3 ligase Parkin regulates neuronal Ca(V)1.3 channel functional expression. *J. Neurophysiol.* **128**, 1555–1564 (2022).
38. F. D. Gregory et al., Harmonin inhibits presynaptic Cav1.3 Ca(2)(+) channels in mouse inner hair cells. *Nat. Neurosci.* **14**, 1109–1111 (2011).
39. B. Liss, J. Striessnig, The potential of L-type calcium channels as a drug target for neuroprotective therapy in Parkinson's disease. *Annu. Rev. Pharmacol. Toxicol.* **59**, 263–289 (2019).
40. D. M. Ramos, W. C. Skarnes, A. B. Singleton, M. R. Cookson, M. E. Ward, Tackling neurodegenerative diseases with genomic engineering: A new stem cell initiative from the NIH. *Neuron* **109**, 1080–1083 (2021).
41. C. Wang et al., Scalable production of iPSC-derived human neurons to identify tau-lowering compounds by high-content screening. *Stem Cell Rep.* **9**, 1221–1233 (2017).
42. M. S. Fernandopulle et al., Transcription factor-mediated differentiation of human iPSCs into neurons. *Curr. Protoc. Cell Biol.* **79**, e51 (2018).
43. E. Bressan, A. Dhingra, S. Donato, P. Heutink, Optimized Derivation of Midbrain Dopaminergic Neurons from iPSCs for research application. *Protocols.io*, 10.17504/protocols.io.bsq5ndy6 (2021).
44. A. J. Hulme, S. Maksour, M. St-Clair Glover, S. Miellet, M. Dottori, Making neurons, made easy: The use of Neurogenin-2 in neuronal differentiation. *Stem Cell Rep.* **17**, 14–34 (2022).
45. P. De Camilli, R. Cameron, P. Greengard, Synapsin I (protein I), a nerve terminal-specific phosphoprotein. I. Its general distribution in synapses of the central and peripheral nervous system demonstrated by immunofluorescence in frozen and plastic sections. *J. Cell Biol.* **96**, 1337–1354 (1983).
46. T. Caspary, C. E. Larkins, K. V. Anderson, The graded response to Sonic hedgehog depends on cilia architecture. *Dev. Cell* **12**, 767–778 (2007).
47. R. Tian et al., CRISPR interference-based platform for multimodal genetic screens in human iPSC-derived neurons. *Neuron* **104**, 239–255.e12 (2019).
48. E. Sipos, S. Komoly, P. Acs, Quantitative comparison of primary cilia marker expression and length in the mouse brain. *J. Mol. Neurosci.* **64**, 397–409 (2018).
49. A. Sterpka, X. Chen, Neuronal and astrocytic primary cilia in the mature brain. *Pharmacol. Res.* **137**, 114–121 (2018).
50. F. F. Kersten et al., Association of whirlin with Cav1.3 (alpha1D) channels in photoreceptors, defining a novel member of the usher protein network. *Invest. Ophthalmol. Vis. Sci.* **51**, 2338–2346 (2010).
51. X. Jin et al., L-type calcium channel modulates cystic kidney phenotype. *Biochim. Biophys. Acta* **1842**, 1518–1526 (2014).
52. X. Jin et al., Cilioplasm is a cellular compartment for calcium signaling in response to mechanical and chemical stimuli. *Cell Mol. Life Sci.* **71**, 2165–2178 (2014).
53. I. Korkka et al., Functional voltage-gated calcium channels are present in human embryonic stem cell-derived retinal pigment epithelium. *Stem Cells Transl. Med.* **8**, 179–193 (2019).
54. G. M. Sanchez et al., The beta-cell primary cilium is an autonomous Ca2+ compartment for paracrine GABA signaling. *J. Cell Biol.* **222**, e202108101 (2023).
55. L. Shi, M. L. Ko, G. Y. Ko, Retinoschisin facilitates the function of L-type voltage-gated calcium channels. *Front. Cell Neurosci.* **11**, 232 (2017).
56. S. R. Shinde, A. R. Nager, M. V. Nachury, Ubiquitin chains earmark GPCRs for BBSome-mediated removal from cilia. *J. Cell Biol.* **219**, e202003020 (2020).
57. P. B. Desai, M. W. Stuck, B. Lv, G. J. Pazour, Ubiquitin links smoothened to intraflagellar transport to regulate Hedgehog signaling. *J. Cell Biol.* **219**, e201912104 (2020).
58. M. Fujimuro, H. Yokosawa, Production of antipolyubiquitin monoclonal antibodies and their use for characterization and isolation of polyubiquitinated proteins. *Methods Enzymol.* **399**, 75–86 (2005).
59. A. K. Ganga et al., Rab34 GTPase mediates ciliary membrane formation in the intracellular ciliogenesis pathway. *Curr. Biol.* **31**, 2895–2905.e7 (2021).
60. C. Spalluto, D. I. Wilson, T. Hearn, Evidence for reciliation of RPE1 cells in late G1 phase, and ciliary localisation of cyclin B1. *FEBS Open Bio.* **3**, 334–340 (2013).
61. T. D. Nguyen, M. E. Truong, J. F. Reiter, The intimate connection between lipids and Hedgehog signaling. *Front. Cell Dev. Biol.* **10**, 876815 (2022).
62. A. Molla-Herman et al., The ciliary pocket: An endocytic membrane domain at the base of primary and motile cilia. *J. Cell Sci.* **123**, 1785–1795 (2010).
63. F. Ye, A. R. Nager, M. V. Nachury, BBSome trains remove activated GPCRs from cilia by enabling passage through the transition zone. *J. Cell Biol.* **217**, 1847–1868 (2018).
64. Z. Anvarian, K. Mykytyn, S. Mukhopadhyay, L. B. Pedersen, S. T. Christensen, Cellular signalling by primary cilia in development, organ function and disease. *Nat. Rev. Nephrol.* **15**, 199–219 (2019).
65. M. V. Nachury et al., A core complex of BBS proteins cooperates with the GTPase Rab8 to promote ciliary membrane biogenesis. *Cell* **129**, 1201–1213 (2007).
66. A. Prasai et al., The BBSome assembly is spatially controlled by BBS1 and BBS4 in human cells. *J. Biol. Chem.* **295**, 14279–14290 (2020).
67. X. Chamling et al., The centriolar satellite protein AZI1 interacts with BBS4 and regulates ciliary trafficking of the BBSome. *PLoS Genet.* **10**, e1004083 (2014).
68. H. Jin et al., The conserved Bardet-Biedl syndrome proteins assemble a coat that traffics membrane proteins to cilia. *Cell* **141**, 1208–1219 (2010).
69. A. R. Nager et al., An actin network dispatches ciliary GPCRs into extracellular vesicles to modulate signaling. *Cell* **168**, 252–263.e14 (2017).
70. A. Bartolome et al., ProteasomeID: Quantitative mapping of proteasome interactomes and substrates for in vitro and in vivo studies. bioRxiv [Preprint] (2022). https://doi.org/10.1101/2022.08.09.503299 (Accessed 9 January 2022).
71. P. Kohli et al., The ciliary membrane-associated proteome reveals actin-binding proteins as key components of cilia. *EMBO Rep.* **18**, 1521–1535 (2017).
72. P. Kiesel et al., The molecular structure of mammalian primary cilia revealed by cryo-electron tomography. *Nat. Struct. Mol. Biol.* **27**, 1115–1124 (2020).
73. F. Farina et al., The centrosome is an actin-organizing centre. *Nat. Cell Biol.* **18**, 65–75 (2016).
74. N. Luo et al., OCRL localizes to the primary cilium: A new role for cilia in Lowe syndrome. *Hum. Mol. Genet.* **21**, 3333–3344 (2012).
75. Y. Rbaibi et al., OCRL1 modulates cilia length in renal epithelial cells. *Traffic* **13**, 1295–1305 (2012).
76. B. G. Coon et al., The Lowe syndrome protein OCRL is involved in primary cilia assembly. *Hum. Mol. Genet.* **21**, 1835–1847 (2012).
77. S. Schmidt et al., Primary cilia and SHH signaling impairments in human and mouse models of Parkinson's disease. *Nat. Commun.* **13**, 4819 (2022).
78. L. Djenoune et al., Cilia function as calcium-mediated mechanosensors that instruct left-right asymmetry. *Science* **379**, 71–78 (2023).
79. S. Yuan, L. Zhao, M. Brueckner, Z. Sun, Intraciliary calcium oscillations initiate vertebrate left-right asymmetry. *Curr. Biol.* **25**, 556–567 (2015).
80. M. Delling, P. G. DeCaen, J. F. Doerner, S. Febvay, D. E. Clapham, Primary cilia are specialized calcium signalling organelles. *Nature* **504**, 311–314 (2013).
81. J. F. Reiter, M. R. Leroux, Genes and molecular pathways underpinning ciliopathies. *Nat. Rev. Mol. Cell Biol.* **18**, 533–547 (2017).
82. N. Mohd Rafiq, Parkinsonism Sac domain mutation in Synaptojanin-1 affects ciliary properties in iPSC-derived dopaminergic neurons [Data set]. Zenodo. https://doi.org/10.5281/zenodo.10797936. Deposited 8 March 2024.